JOURNAL OF MATERIALS SCIENCE: MATERIALS IN MEDICINE **8** (1997) 325–332

Physico-chemistry and cytotoxicity of ceramics

Part I *Characterization of ceramic powders*

I. DION, F. ROUAIS, Ch. BAQUEY
INSERM U. 443 and Laboratoire de Biophysique, Université de Bordeaux II, 146 rue Léo Saignat, 33076 Bordeaux Cedex, France
TERACOR, ZI Toulon-Est, BP 238, 80 Avenue Lagrange, 83089 Toulon Cedex, France

M. LAHAYE
Département de Microanalyse, Université de Bordeaux I, 351, Cours de la Libération, 33405 Talence Cedex, France

R. SALMON, L. TRUT, J. P. CAZORLA
Laboratoire de Chimie du Solide, CNRS, Université de Bordeaux I, 351, Cours de la Libération, 33405 Talence Cedex, France

P. V. HUONG
Laboratoire de Spectroscopie Moléculaire et Cristalline, Université de Bordeaux I, Cours de la Libération, 33405 Talence Cedex, France

J. R. MONTIES, P. HAVLIK
LRC, Université Aix-Marseille II, Avenue Jean-Moulin, 13385 Marseille Cedex, France

The morphology of Al_2O_3, ZrO_2/Y_2O_3, AlN, B_4C, BN, SiC, Si_3N_4, TiB_2, TiC, TiN ceramic, graphite and diamond powders has been studied by scanning electron microscopy (SEM) and the specific area of each powder was determined with the BET method. X-ray diffraction (XRD) investigations have been carried out in order to evaluate the crystallinity and determine the constitutive phases. The chemical composition was assessed by classical chemical analyses and by X-ray microprobe; some powders were studied by the laser micro-Raman technique. Correlations have been established between all these results.

1. Introduction
Ceramic materials are expected to become the "new biomaterials" for blood-contacting applications, either as ceramic coatings deposited on substrates or as bulk ceramics. Furthermore, uncommon ceramic materials could be candidates in other biomedical applications such as in orthopaedic surgery. The purpose of this global study is to characterize ceramic powders with several techniques already described [1] before evaluating their cytotoxicity and their cytocompatibility.

2. Materials and methods
2.1. Ceramic powders
Alumina (Al_2O_3), zirconium oxide/yttrium oxide (ZrO_2/Y_2O_3) and silicon carbide (SiC) were supplied by Lonza France – Martinswerk GmbH. Aluminium nitride (AlN), boron carbide (B_4C), boron nitride (BN) and titanium diboride (TiB_2) were provided by Comaip-ESK. Titanium carbide (TiC) and titanium nitride (TiN) were purchased from CEREX. Diamond powder was elaborated by De Beers Industrial Diamond Division-Eskenazi SA and graphite powder was supplied by Superior Graphite Co.

2.2. Scanning electron microscopy
The scanning electron microscopy (SEM) used here was a Hitachi S 2500. All powders were metallized by gold. The magnification varies from 50 to 50 000, at 15 or 20 kV, depending on the nature of the powders. Some powders were examined as tablets coated with carbon and other ceramic powders were deposited on an indium (In) film to allow the observations.

2.3. X-ray diffraction analysis
The X-ray diffractometer was a Philips PW 1050 Spectrogoniometer (CuK_{α_1}, $\lambda = 1.5405$). Each powder was deposited on an aluminium plate.

2.4. X-ray microprobe
The X-ray microprobe apparatus used here was a Camebax-Tracor system. Some powder tablets were

coated with carbon and some ceramic powders were deposited on an indium (In) film to allow the elemental analysis.

2.5. Laser micro-Raman spectroscopy
The Raman spectra were recorded on a micro-spectrophotometer Dilor Omars 89 fitted out with a multichannel detector of 1024 photodiodes and a Spectra Physics 164 laser source the emission of which is 514.5 nm and 488.0 nm. The spatial resolution was about 1 μm^2.

2.6. BET specific areas
All powders specific areas were assessed on a physical adsorption analyser Micromeritics using the BET method (Fig. 29).

3. Results
3.1. Scanning electron microscopy
Al_2O_3 (Fig. 1) and BN (Fig. 5) powders show a sticked plate-like morphology. ZrO_2/Y_2O_3 (Fig. 2) and TiC (Fig. 9) are submicronic ultrafine spheroidal particles. AlN (Fig. 3) is composed of particles of various sizes and shapes. SiC (Fig. 6), B_4C (Fig. 4) and diamond (Fig. 12) particles are angular while Si_3N_4 (Fig. 7), TiB_2 (Fig. 8) and TiN (Fig. 10) present irregular shapes. Graphite particles (Fig. 11) are nodular.

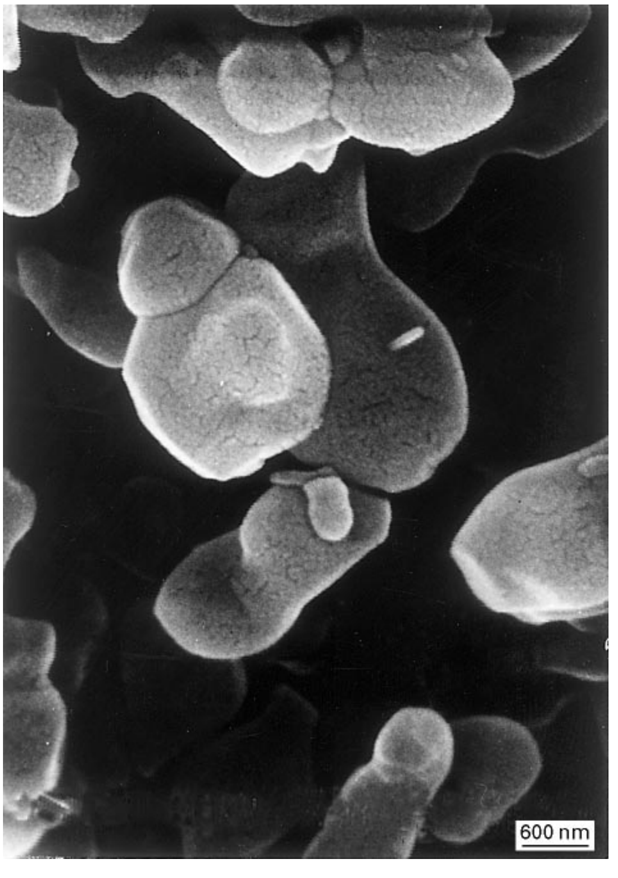

Figure 1 SEM Al_2O_3.

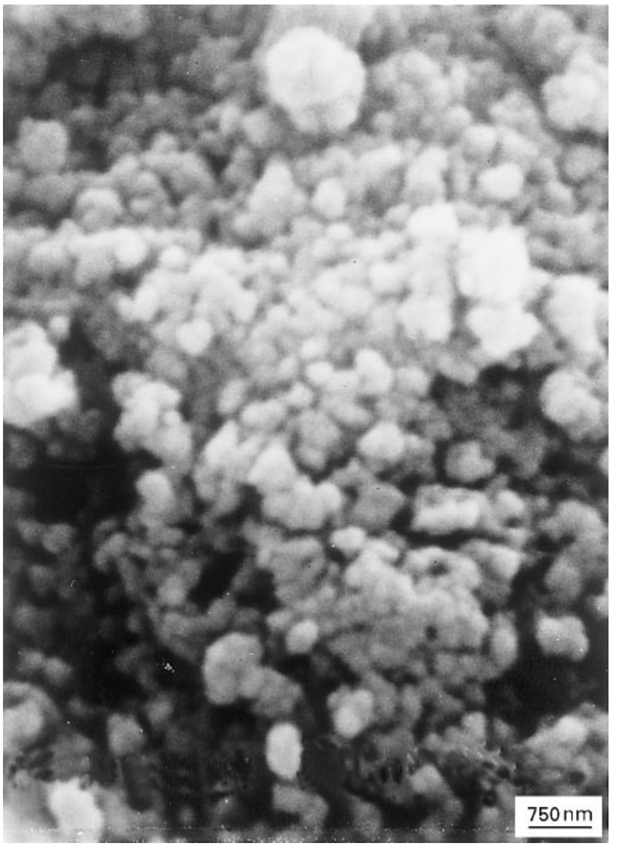

Figure 2 SEM ZrO_2/Y_2O_3.

Figure 3 SEM AlN.

3.2. X-ray diffraction
Al_2O_3 (Fig. 13) is pure α-alumina with a trigonal lattice. ZrO_2 (Fig. 14) is present both in monoclinic

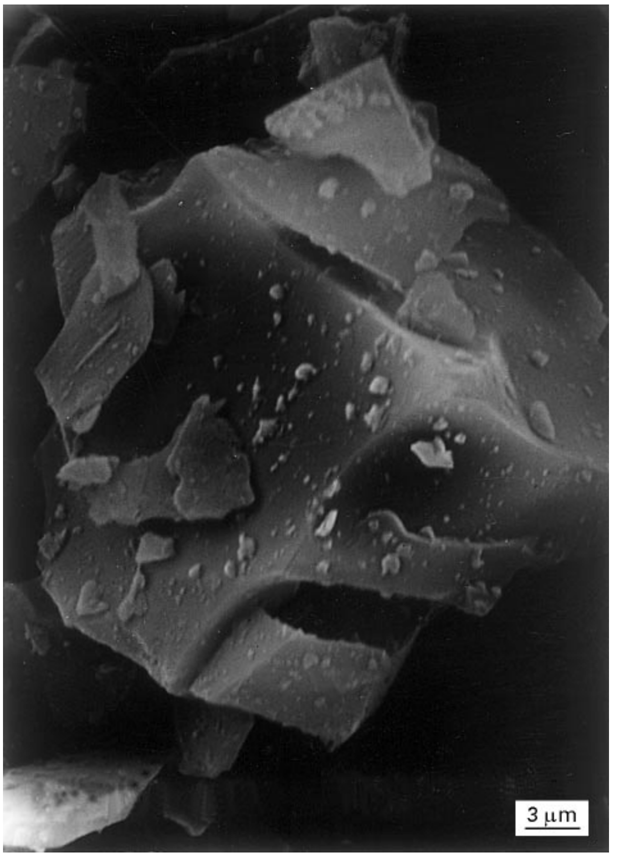

Figure 4 SEM B_4C.

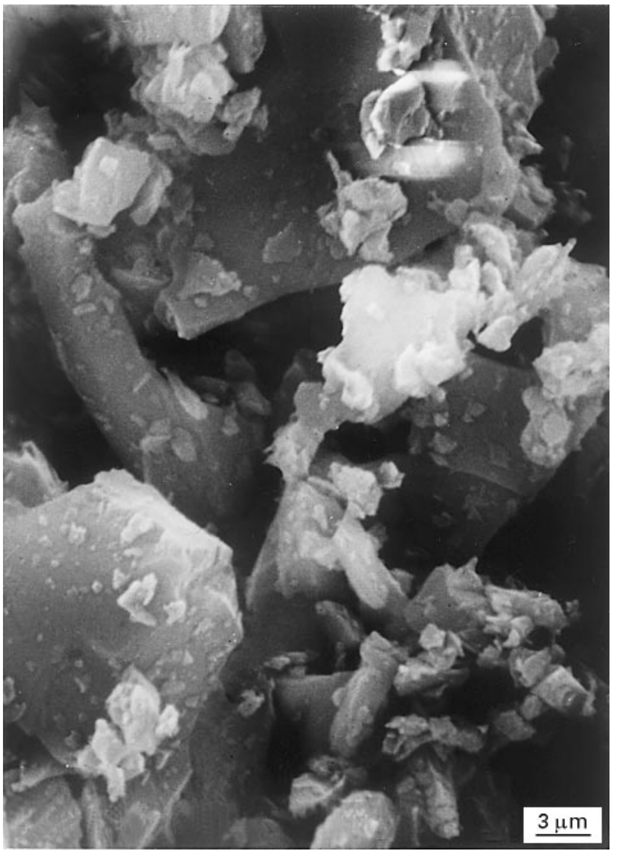

Figure 6 SEM SiC.

Figure 5 SEM BN.

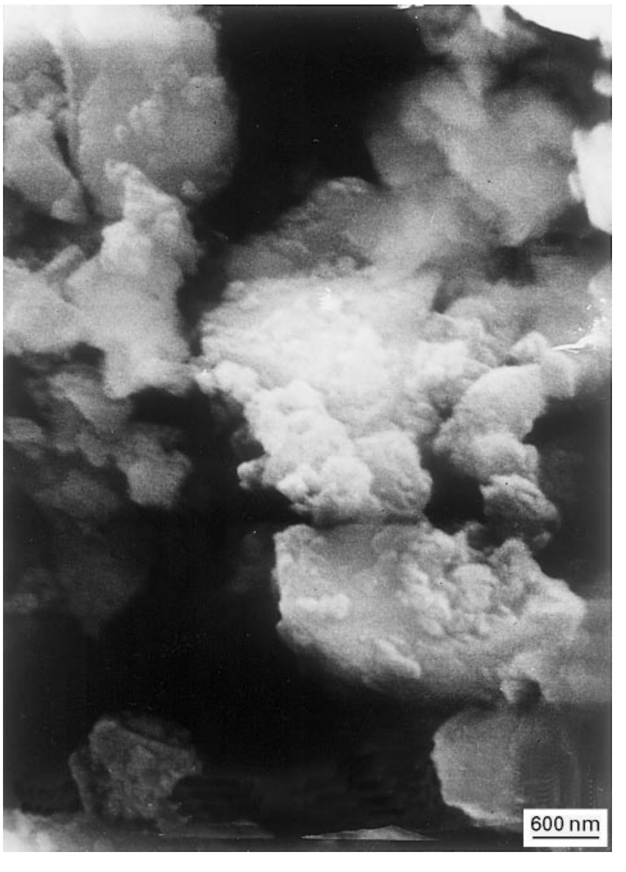

Figure 7 SEM Si_3N_4.

and tetragonal systems. AlN (Fig. 15), B_4C (Fig. 16), BN (Fig. 17), Si_3N_4 (Fig. 19), TiB_2 (Fig. 20) and graphite (Fig. 23) show a hexagonal structure, they are all pure and (AlN) 4H, (BN) 4H, (Si_3N_4) 28H and (TiB_2) 3H are present, respectively, instead of AlN, BN, Si_3N_4 and TiB_2. TiC (Fig. 21), TiN (Fig. 22) and diamond (Fig. 24) present a cubic lattice, TiC and TiN are pure while diamond is mixed with ZrO_2

Figure 8 SEM TiB_2.

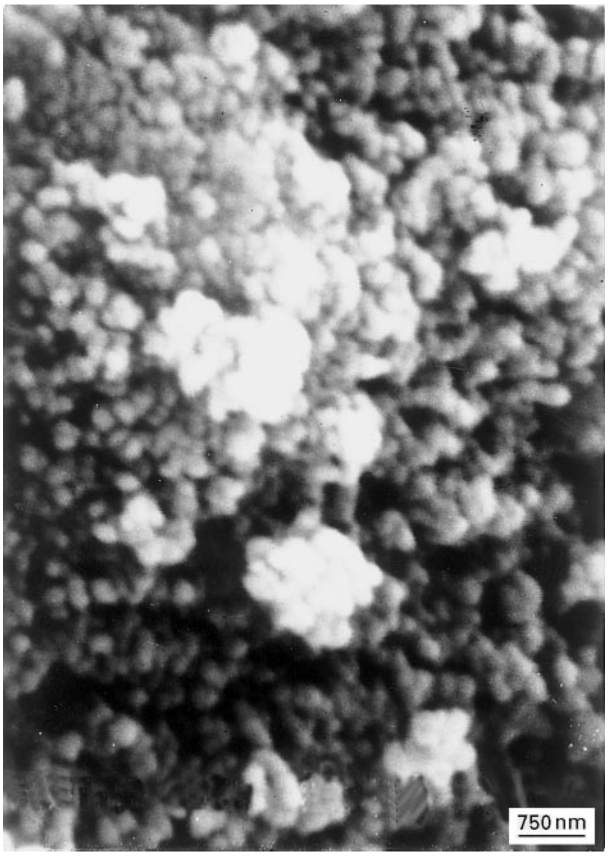

Figure 9 SEM TiC.

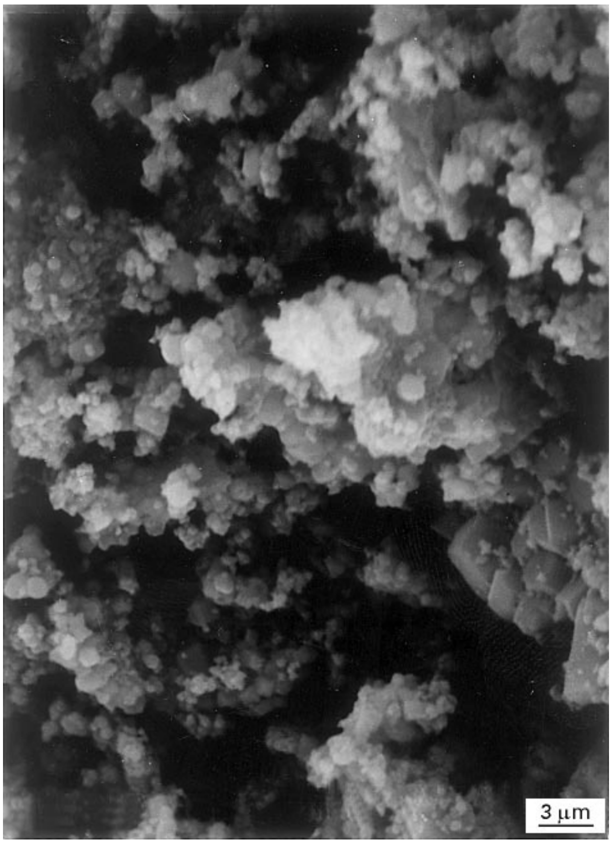

Figure 10 SEM TiN.

Figure 11 SEM graphite.

Figure 12 SEM diamond.

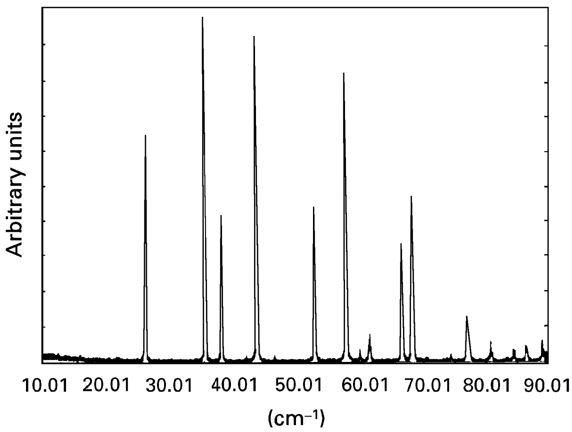

Figure 13 XRD Al_2O_3.

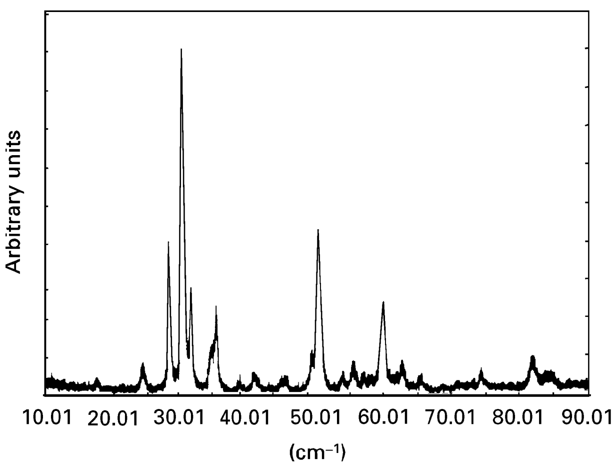

Figure 14 XRD ZrO_2/Y_2O_3.

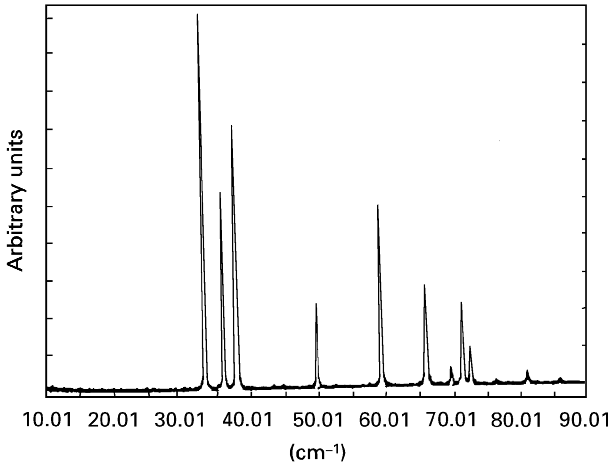

Figure 15 XRD (AlN) 4H.

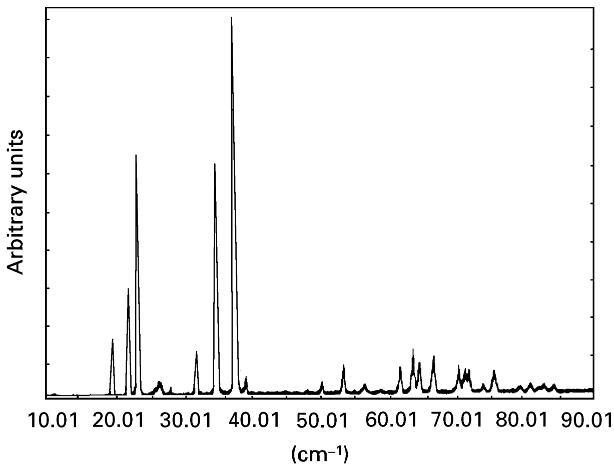

Figure 16 XRD B_4C.

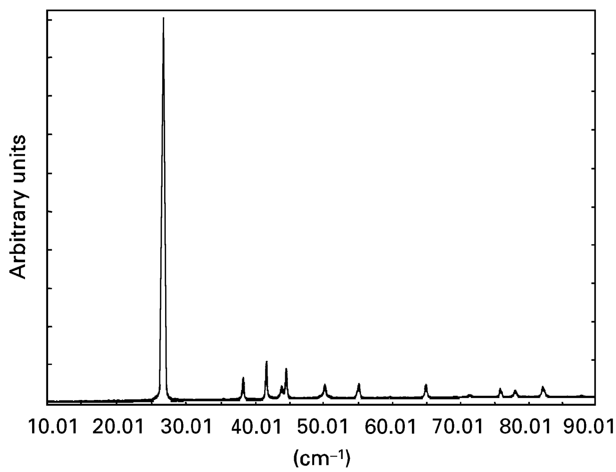

Figure 17 XRD (BN) 4H.

(tetragonal structure). The SiC phase (Fig. 18) is an α-phase with a rhombohedral structure.

3.3. Chemical composition

Table I shows the chemical composition of all powders. On the left, the values represent the chemical analysis carried out by the suppliers and the figures given on the right of the table result from the X-ray microprobe assay (neither light elements H, Li, B, Be, C, N, O, F, nor some halogens could be detected with this facility).

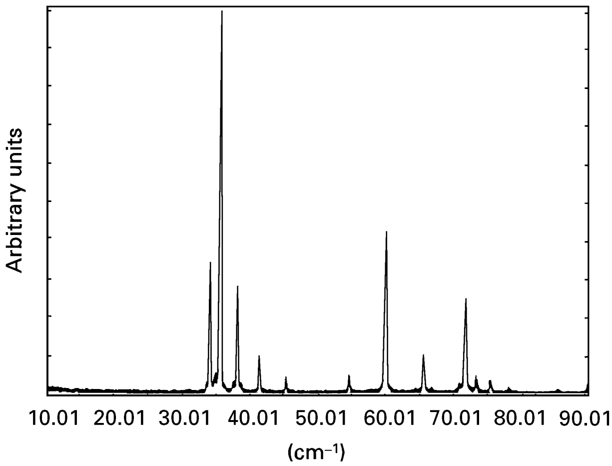

Figure 18 XRD SiC.

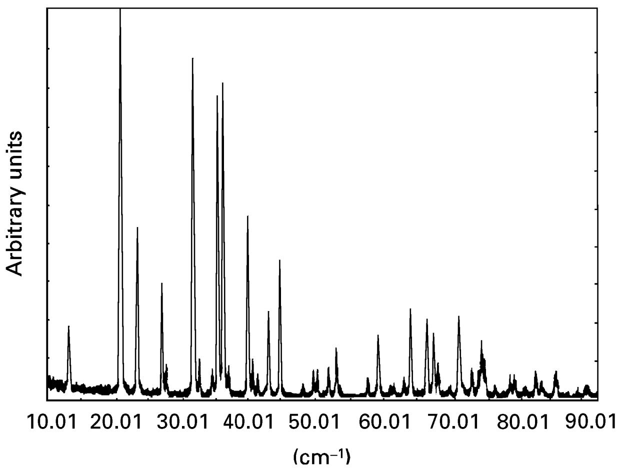

Figure 19 XRD (Si_3N_4) 28H.

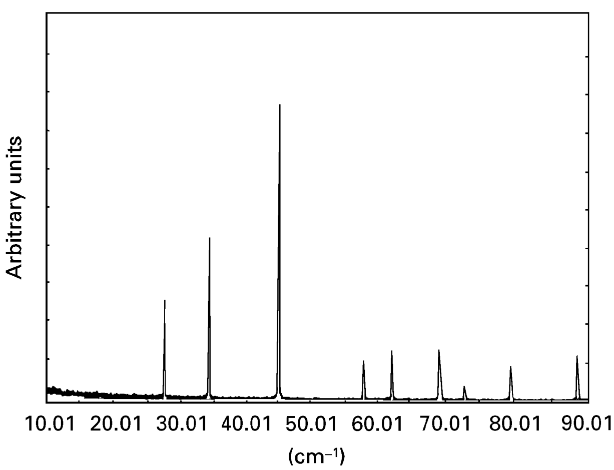

Figure 20 XRD (TiB_2) 3H.

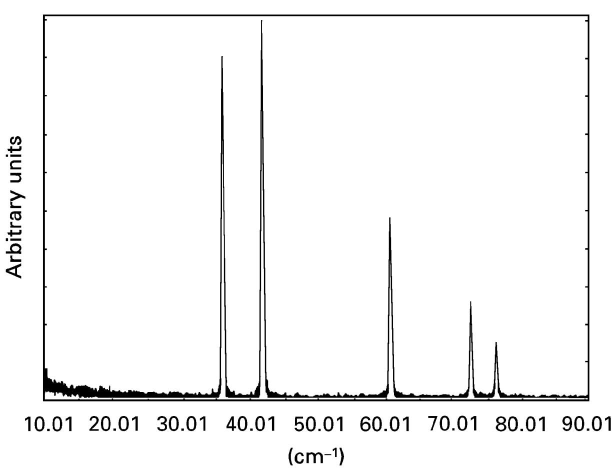

Figure 21 XRD TiC.

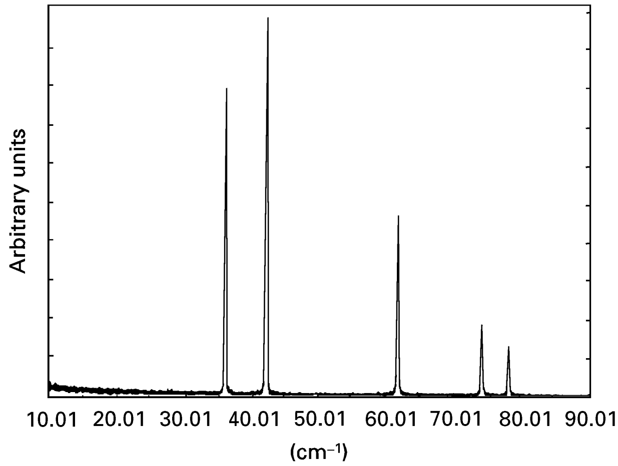

Figure 22 XRD TiN.

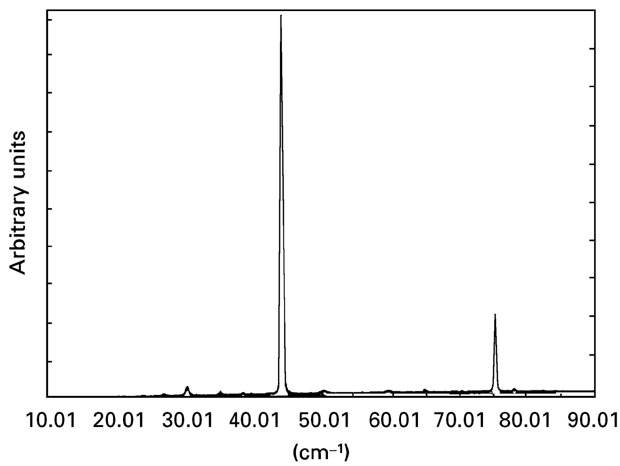

Figure 23 XRD diamond.

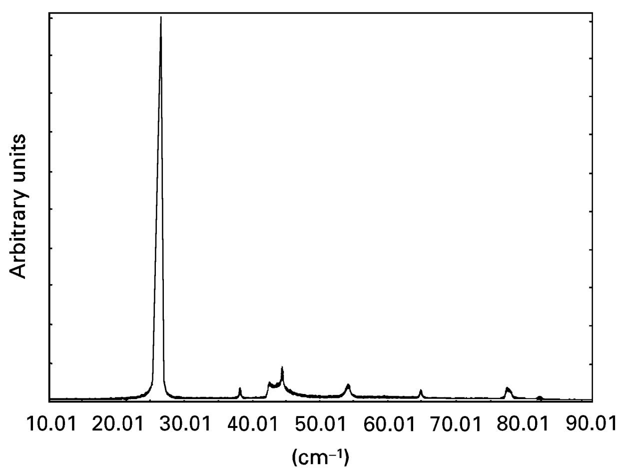

Figure 24 XRD graphite.

3.4. Laser micro-Raman spectroscopy

Zirconia is represented in Fig. 25 by the main peaks. The peak at 380 cm^{-1} is characteristic of Y_2O_3. As the ZrO_2 structure is still crystalline, we can say that the yttrium oxide percentage is low – about 5%.

Alumina is represented by two characteristic peaks at 379.6 cm^{-1} and 418.1 cm^{-1} (Fig. 26).

Natural diamond has been detected having two structures, the most common being the cubic one (Fig. 27); the other structure, "hexagonal diamond" (Fig. 28) has a narrow band at 1322 cm^{-1} [2, 3].

TABLE I Chemical composition of powders (wt %)

Powder	Chemical composition (wt %)			Trace elements (wt %)
Al_2O_3	Al_2O_3	min	99.99	
	Na_2O_3	max	0.0030	
	K_2O	max	0.0010	
	CaO	max	0.0005	
	MgO	max	0.0008	
	Fe_2O_3	max	0.0012	
	Cr_2O_3	max	0.0004	
	SiO_2	max	0.0050	
ZrO_2/Y_2O_3	ZrO_2		93.06	
	Y_2O_3		5.3	
	TiO_2		0.10	
	HfO_2		1.4	
	SiO_2		0.1	
	Al_2O_3		0.02	
	Fe_2O_3		0.01	
	MgO	max	0.01	
	Cl	max	0.10	
AlN	Al	min	30.8	
	N	min	63.5	
	O	max	3.0	
	metal.	impur. max	0.8	Fe 0.2
B_4C	B	min	76.0	
	C	min	19.5	
	B_2O_3	max	0.6	
	Fe	max	0.2	
	O	max	1.0	
	N	max	1.0	
	Si	max	0.15	Si: 0.05
				Ti: 0.02
BN	BN	min	98.5	
	N_2	min	54.5	
	B	min	43.0	
	O	max	1.5	
	B_2O_3	max	0.1	
	C	max	0.1	
	metal.	impur. max	0.2	
				Si: 0.05
				S: 0.05
				Co: 0.02
				Ta: 0.05
SiC	Free C		0.19	
	Free Si		0.08	
	O		0.34	
	Al		0.03	Al: 0.02
	Fe		0.05	Fe: 0.15
	Ti		0.02	
	Na		0.015	
	W	max	0.01	
	Co	max	0.01	
	Mg	max	0.005	
	Ca	max	0.006	
	N	max	0.008	
Si_3N_4	Free Si	max	0.1	
	N		38.43	
	C		0.17	
	O		1.90	
	Fe		0.013	
	Al		0.035	Al: 0.02
	Ca		0.004	
				Ti: 0.05
TiB_2	Ti	min	66.5	
	B	min	30.5	
	C	max	0.5	
	B_2O_3	max	0.5	
	O	max	0.5	
	N	max	0.5	
	Fe	max	0.2	Fe: 0.15
				Ca: 0.20
				Pt: 0.06
TiC	Ti		78.2	
	N		0.12	
	O		2.08	
	C		19.03	
	Fe		0.79	Fe: 0.40
	Ca		0.23	Ca: 0.60
				Al: 0.40
				S: 0.10
				Cl: 0.20
TiN	Ti		77.5	
	N		21.2	
	O		0.93	
	Fe		0.37	Fe: 0.20
	Ca		0.133	Ca: 0.05
				K: 0.03
				Cl: 0.10
				Al: 0.04
Diamond	C			Al: 0.05
				Si: 0.15
				Fe: 0.05
				Zr: 1.00
Graphite	C		99.99	
	S		0.01–0.03	S: 0.03
				K: 0.05
				Fe: 0.04

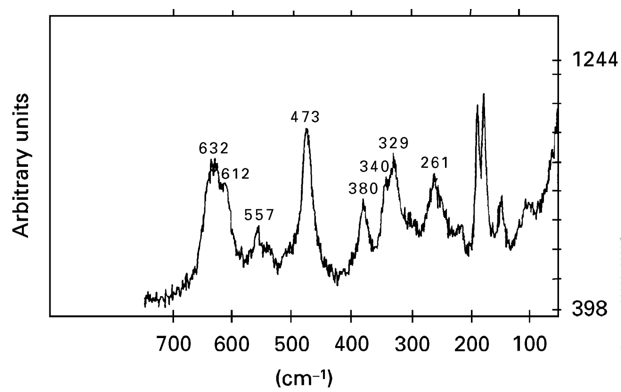

Figure 25 Laser micro-Raman spectra of ZrO_2/Y_2O_3.

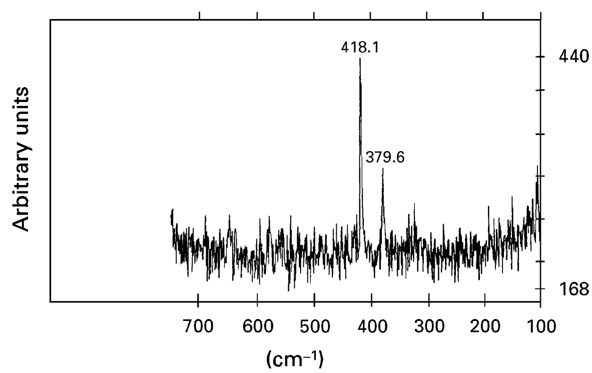

Figure 26 Laser micro-Raman spectra of Al_2O_3.

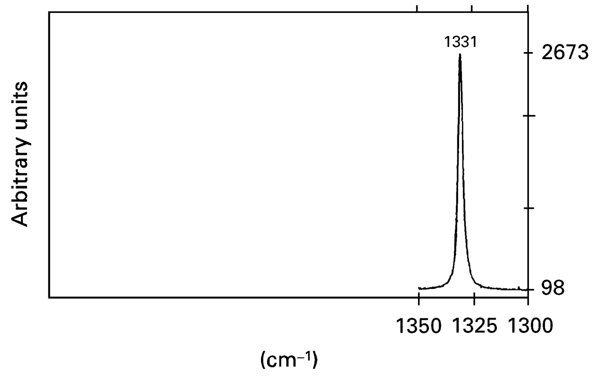

Figure 27 Laser micro-Raman spectra of diamond (cubic structure).

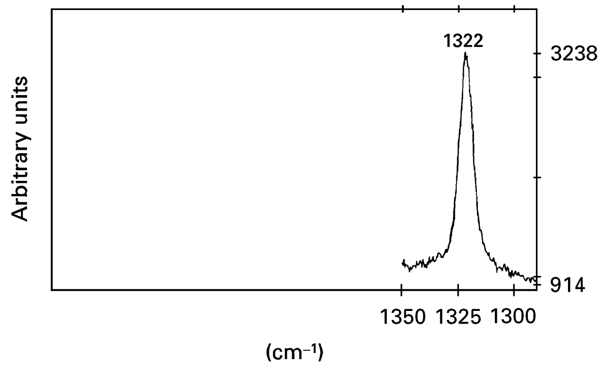

Figure 28 Laser micro-Raman spectra of diamond (hexagonal structure).

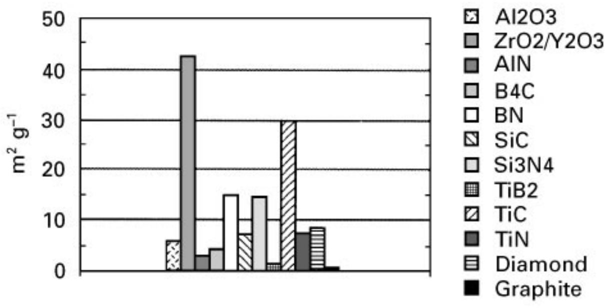

Figure 29 Histogram of BET specific areas.

TABLE II BET specific areas ($m^2 g^{-1}$)

Sample powder	BET specific surface ($m^2 g^{-1}$)
Al_2O_3	5.855 ± 0.006
ZrO_2/Y_2O_3	42.5940 ± 0.0002
AlN	3.041 ± 0.006
B_4C	4.298 ± 0.008
BN	15.054 ± 0.003
SiC	7.027 ± 0.003
Si_3N_4	14.6220 ± 0.0009
TiB_2	1.34 ± 0.01
TiC	29.75900 ± 0.00006
TiN	7.610 ± 0.004
Diamond	8.522 ± 0.002
Graphite	0.71 ± 0.05

3.5. BET specific areas

Table II shows the various values of specific areas.

4. Discussion and conclusions

All powders are crystalline and their purity varies from 93 to 99.99% or more.

Many shapes are present and some powders such as zirconia (X-ray diffraction) and diamond (micro-Raman spectroscopy) show more than one structure.

Concerning the elemental chemical composition, the suppliers gave average composition values of the powders. As a batch from several available was used, some slight differences were noticed. Moreover, their composition values for trace elements are given with a security margin and are indexed under maximal values. This is the reason why trace elements were found with lower concentrations, except for two of them, by the X-Ray microprobe technique. The microprobe facility allowed the detection of exotic contaminants not usually looked for, such as Co, Pt, Zr etc. Some elements which were present in too small quantities to be seen by this technique were detected by classical titrations.

X-ray diffraction and X-ray microprobe techniques showed a contamination of diamond by Zr (ZrO_2). Using laser micro-Raman spectroscopy it was shown that diamond presents the known cubic structure but also an unusual hexagonal lattice.

However, there is good correlation between chemical compositions given by X-ray diffraction chemical analyses and micro-Raman spectroscopy. This could be expected as all these techniques are complementary.

Acknowledgements

The authors would like to thank M. O. Rubio for her photographic work and V. Silverio for typing the manuscript.

References

1. M. AMMOU, *CRAM-CNRS* (1989).
2. P. V. HUONG, B. MARCUS, M. MERMOUX, D. K. VEIRS and G. M. ROSENBLATT, *Diamond and Related Materials B* **1** (1992) 1.
3. P. V. HUONG, *Mater. Sci. Engng. B* **11** (1991) 235.

Received 19 June 1992
and accepted 12 January 1993